An Effective Compensation Technique for Speed Smoothness at Low-Speed Operation of PMSM Drives

Azeddine Houari, Ahmed Bouabdallah, Ali Djerioui, Mohamed Machmoum, Francois Auger, Abdallah Darkawi, Jean-Christophe Olivier, and Mohamed Fouad Benkhoris

***Abstract*—This paper proposes a simple and effective method to reduce speed ripples of permanent magnet synchronous machines (PMSMs) under low-speed working conditions. The treated issue is related to the periodic torque ripples, which induce speed oscillations that deteriorate the drive performance. The main idea of the proposed method is to modify a conventional PMSM controller by superposing an appropriate compensation signal to the quadratic-current reference. The proposed approach allows the reduction of speed ripples at low speed through a simple compensation signal and does not require a hard calculation cost. A theoretical analysis is presented, and both simulation and experimental results are presented to validate the proposed compensation method.**

***Index Terms*—Low-speed operation, permanent magnet synchronous machine (PMSM), speed ripple reduction.**

I. Introduction

PERMANENT magnet synchronous machines (PMSMs) are still favored for several applications such as high-performance servo applications, robotics, and mechatronics, due to their advantages: 1) high efficiency; 2) high reliability; 3) high torque-to-inertia ratio; and 4) fast dynamics [1], [2]. However, the main drawback of PMSM drives is the existence of parasitic torque ripples under low-speed working conditions. This phenomenon can owe from the machine design imperfectness, the measurements uncertainties, and the interaction between the PMSM and the mechanical load or power electronic devices. These ripples severely degrade the speed control performance and can also lead to mechanical vibrations and acoustic noises [2]. The pulsating torque can be separated into both low-frequency and high-frequency components. While the high-frequency components can effectively be limited by increasing the bandwidth of the control loops, the low-frequency ones occur within the bandwidth of the controller and need special attention [3].

Regarding the popularity of this kind of machine in industrial applications, periodic torque ripple reduction has received much attention in recent years, and different techniques have been presented throughout the literature. Two groups of techniques can be distinguished. One is focusing on the improvement of the machine design [4] and the other intends to reduce the torque ripple effect by using advanced control algorithms [5]. The design optimization is a natural way to reduce the torque ripple phenomenon. However, practical optimization of the machine design results in higher costs and more complicated realization. A common approach for torque ripple reduction is the harmonic cancellation using the current profiling. Numerous control approaches to cancel the torque harmonics have been presented in the literature [6]–[23]. For example, in [6], two periodic speed ripple minimization schemes using iterative learning control (ILC) are presented and compared. It is shown that the learning control scheme implemented in the frequency domain is more efficient than the one implemented in the time domain. Adding to the proper machine nonlinearities, the effect of the induced pulsating torque by the load is illustrated. In [7], the authors underline that iterative learning controllers can produce infinite gains at a series of frequencies and achieve accurate reference tracking and total disturbance rejection, but at the same time, they may bring instability risks, particularly when they are used in speed loop. A speed and current proportional-integral-resonant (PIR) control strategy is proposed to minimize the periodic torque ripples. The proposed method considers the nonideal factors (flux harmonics, cogging torque, etc.) in the controller design. However, the resonant term design is strongly related to a specific perturbation. So, if a large disturbance of the frequency occurs, the PIR control will no more correctly reject the perturbation. In [8], the disturbance frequency arising from current sensor offset errors is embedded in the design of

Manuscript received June 17, 2016; revised September 30, 2016; accepted November 13, 2017. Date of publication August 16, 2017; date of current version January 18, 2018. Paper 2016-IACC-0543.R1, presented at the 2015 IEEE Industry Applications Society Annual Meeting, Addison, TX, USA, Oct. 18–22, and approved for publication in the IEEE Transactions on Industry Applications by the Industrial Automation and Control Committee of the IEEE Industry Applications Society. *(Corresponding author: Azeddine Houari.)*

A. Houari, A. Bouabdallah, M. Machmoum, F. Auger, A. Darkawi, J.-C. Olivier, and M.-F. Benkhoris are with the Institut de Recherche en Energie Electrique de Nantes Atlantique, Saint-Nazaire 44602, France (e-mail: azeddine.houari@univ-nantes.fr; ahmed.bouabdallah@univ-nantes.fr; Mohamed.Machmoum@univ-nantes.fr; francois.auger@univ-nantes.fr; Abdallah.Darkawi@univ-nantes.fr; jean-christophe.olivier@univ-nantes.fr; Mohamed-Fouad.Benkhoris@univ-nantes.fr).

A. Djerioui is with the Institut de Recherche en Energie Electrique de Nantes Atlantique, Saint-Nazaire 44602, France, and also with the Department of Electrical Engineering, Faculty of Technology, University of Mohamed Boudiaf, M'sila 28000, Algeria (e-mail: ali.djerioui@etu.univ-nantes.fr).

Color versions of one or more of the figures in this paper are available online at http://ieeexplore.ieee.org.

Digital Object Identifier 10.1109/TIA.2017.2740388

a model-predictive-based controller to minimize the speed ripples. Also, in [9], the measurement offsets and unequal sensor gains, which are possible reasons for unbalanced phase currents, are compensated by a phase current reconstruction strategy. In [10], an improved torque predictive control is proposed to reduce the torque ripple and to enhance the system dynamics. The main idea is to include both the torque and stator-flux error information in the control calculation. These kinds of controls necessitate the use of high-performance processors in order to properly solve the optimization problem. In [11], the effect of unbalanced stator resistances in the torque ripple is investigated. It was shown that the estimated values of these resistances could be used to compensate the high-frequency components of the torque ripple. In [12], the proposed torque ripple reduction is based on instantaneous torque estimation with a rigorous analytical model that takes spatial harmonics into account. The work presented in [13] calculates the best current, which minimizes the torque oscillation by the use of learning capabilities of an adaptive linear network algorithm. The main disadvantage of these methods is their real-time implementation complexity in industrial applications.

In this paper, an effective compensation technique is proposed to ensure speed smoothness at low-speed operation of PMSM drives. The approach is based on the injection of a compensating signal in a conventional field-oriented control (FOC). This is done in order to use the low-frequency current disturbance, which is usually within the bandwidth of the controller to modify the main reference current in such a way that the undesired disturbing signal is rejected by the controller. The design procedure of the proposed speed ripple compensator takes the local stability of the system, the disturbance rejection, and the robustness under the parametric variations into account. The proposed technique can present an advantage from an industrial point of view, where the implementation cost is important. In fact, the proposed algorithm is added to a classical speed-oriented control algorithm and is composed of a high-pass filter in series with a gain. Compared to learning-, observation-, and optimization based-approaches, where design procedures are complex and need heavy computational capability to ensure proper real-time calculation, the proposed technique is simpler to synthesis and does not require a high calculation cost.

The remainder of this paper is presented as follows. A description of the studied system and its control is presented in Section II. In Section III, the design principle of the proposed compensation method is provided. Section IV presents simulation results. In Section V, experimental results validate the effectiveness of the proposed compensation technique. Finally, Section VI underlines the contributions of this work.

II. System Modeling and Control

A. System Description

The studied drive is made of a dc power source, a three-phase inverter, and a nonsalient PMSM. The control part is based on a modified FOC. Its scheme can be divided into two blocks: the speed regulator block based on a cascaded proportional integral (PI) loop and the speed ripple compensator block (see Fig. 1).

B. PMSM Model

The electrical model of a nonsalient PMSM in the synchronous Park reference frame is expressed as

$$\mathbf{u_s} = R_s \mathbf{i_s} + \dot{\mathbf{\Psi}}_s + \omega_E \mathbf{J} \mathbf{\Psi}_s \tag{1}$$

where $\mathbf{u_s} = [u_d, u_q]^T$ is the stator voltage vector, $\mathbf{i_s} = [i_d, i_q]^T$ is the stator current vector, $\mathbf{\Psi_s} = [\psi_d, \psi_q]^T$ is the stator flux linkage vector, R_s is the stator per-phase resistance, and ω_E is the electrical angular velocity.

$\mathbf{J} = \begin{bmatrix} 0 & -1 \\ 1 & 0 \end{bmatrix}$ is a coupling matrix. The stator flux can be formulated as follows:

$$\mathbf{\Psi_s} = L_s \mathbf{i_s} + \mathbf{\Psi_{PM}} \tag{2}$$

where $\mathbf{\Psi_{PM}} = [\psi_{\text{PM}}, 0]^T$ is the magnet flux and L_s is the stator inductances. The mechanical equation and the electromagnetic torque are given by

$$\dot{\omega}_E = \frac{p}{J_M} \left(\Gamma_{\text{EM}} - \Gamma_L \right) - \frac{F_M}{J_M} \omega_E \tag{3}$$

$$\Gamma_{\text{EM}} = p \mathbf{\Psi}_s^T \mathbf{J}^T \mathbf{i}_s \tag{4}$$

where Γ_{EM} and Γ_L are, respectively, the electromagnetic and the load torques, F_M is the mechanical frictional coefficient, J_M is the mechanical inertia, and p is the number of pole pairs.

C. Control Strategy

As presented in Fig. 1, the control method is based on cascaded PI loops, i.e., an outer speed loop and an inner current loop. As usual in nonsalient PMSM control, the d-axis current reference i_d^{Ref} is fixed to zero and the quadratic current reference i_q^{Ref} is deduced directly from the speed outer loop. Then, the dq-axis input controls are calculated by using a PI-type decoupling control

$$\mathbf{u_s^{\text{Ref}}} = K_{p_C} \boldsymbol{\epsilon_c} + K_{i_C} \int \boldsymbol{\epsilon_c} dt + \omega_E L_s \mathbf{J} \mathbf{i_s} + \mathbf{J} \mathbf{\Psi_{PM}} \tag{5}$$

where $\mathbf{u_s^{\text{Ref}}} = [u_d^{\text{Ref}}, u_q^{\text{Ref}}]^T$ is the reference input voltages, and $\boldsymbol{\epsilon_c} = [(i_d^{\text{Ref}} - i_d), (i_q^{\text{Ref}} - i_q)]^T$ is the current control error. The controller design is based on a simple pole placement. The bandwidth of the current controller is placed so as to obtain both a fast response time and a good disturbance rejection ability. The resulting control gains are $K_{p_C} = 2\xi L_s \omega_C - R_s$ and $K_{i_C} = L_s \omega_C^2$, where $\xi = 0.7$ and ω_C represent the damping ratio and the cutoff pulsation of the current loop, respectively.

The outer loop controls the velocity of the motor to its reference ω_E^{Ref} and yields the q-axis current reference. The speed control bandwidth is selected in such a manner to ensure the control objective and to avoid interaction between the outer speed and the inner current loops. The speed controller gains $K_{p\omega}$ and $K_{i\omega}$ are equal to $K_{p\omega} = \frac{2\xi J_M \omega_\omega}{p^2 \psi_{\text{PM}}}$ and $K_{i\omega} = \frac{J_M \omega_\omega^2}{p^2 \psi_{\text{PM}}}$, where ω_ω represents the cutoff pulsation of the speed loop.

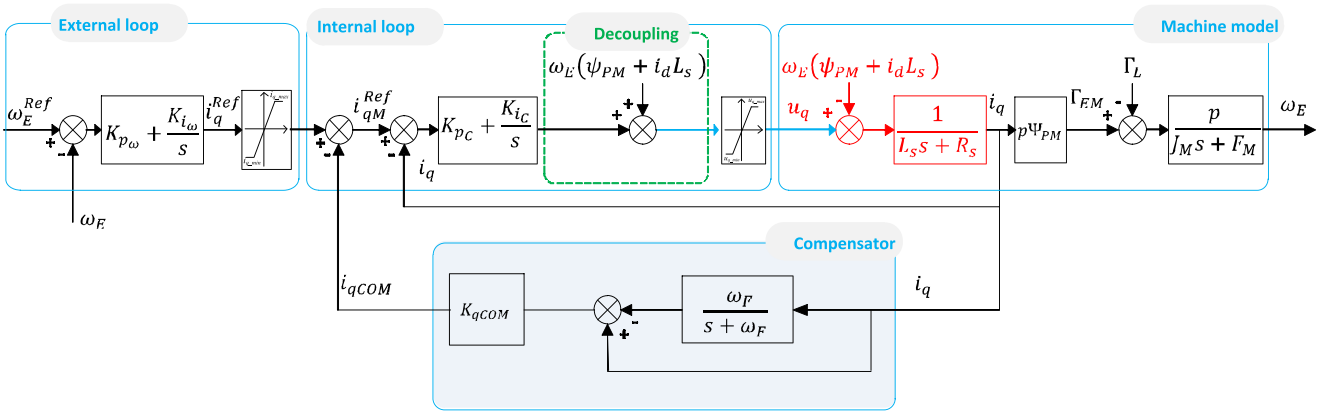

Fig. 1. Overall block diagram of the system with the proposed speed ripple compensator.

D. Low-Frequency Torque Pulsations

The periodic torque ripples can owe from different features that can be combined, and the resulting electromagnetic torque can be expressed as the sum of the main dc component (Γ_{EM_0}) and the harmonic components $(\Delta\Gamma_{\mathrm{EM}})$

$$\Gamma_{\mathrm{EM}} = \Gamma_{\mathrm{EM}_0} + \Delta\Gamma_{\mathrm{EM}}. \tag{6}$$

Various harmonic components are contained in the electromagnetic torque due to many causes, such as harmonics of the motor flux, conditioning causes, sensor offsets, and coupling devices perturbations. These disturbances can be separated into low-frequency and high-frequency components. The high-frequency ripples can be removed by the load inertia or by the bandwidth of the speed control loop, but the low-frequency ripples that occur within the bandwidth could still cause oscillations. The following part illustrates the effect of some disturbances on the emergence of low-order harmonics in the electromagnetic torque.

1) Current Sensor Offset Error: The sensors inaccuracy is related to the presence of inherent dc offsets due to the conversion process between the phase current probe and the input of the controller. DC offsets in stator current measurements cause pulsating torque oscillations at the fundamental frequency [6], which can be described as

$$\Delta\Gamma_{\mathrm{EM}_1} = \beta\cos(\theta_E + \alpha)\sqrt{\Delta i_a^2 + \Delta i_a \Delta i_b + \Delta i_b^2} \tag{7}$$

where Δi_a and Δi_b are the offset errors in the measured phase currents, θ_E is the electrical angle, β is a constant, and α is a constant angle displacement.

2) Gain Mismatch: For conditioning problems, the gain mismatch error arises from the difference between the current sensors gains. This issue causes torque oscillations at twice the fundamental frequency [24], and the resulting oscillation torque can be expressed as

$$\Delta\Gamma_{\mathrm{EM}_2} = \gamma\cos\left(2\theta_E - \frac{2\pi}{3}\right) \tag{8}$$

where γ is a constant, which presents the errors in gains of the current sensors.

3) Flux Harmonics: Another major source of torque pulsation is the periodic flux due to the nonsinusoidal flux density distribution in the air gap. The corresponding torque harmonics appear as the sixth, 12th, and other multiples of the sixth harmonics [6] and can be expressed as

$$\Delta\Gamma_{\mathrm{EM_{FH}}} = \sum_{i=1}^{i=n} A_{6i}\cos(6i\theta_E) \tag{9}$$

where A_{6i} is the magnitude of multiple-torque sixth-harmonic components.

As a result, the various torque ripple factors induce speed oscillation that deteriorates the drive performance.

III. Proposed Speed Ripple Compensator

The aim of this section is to introduce the proposed speed ripple compensator. In order to reduce the speed ripples under low-speed working conditions, the reference value of the q-axis current is modified with respect to the identified current disturbances. So, these low-frequency disturbances are rejected properly by the inner PI loop. The design technique takes the local stability of the system, the disturbance rejection, and the robustness under the parametric variations into account.

This section consists of two parts. First, the compensation principle is presented. Then, the design methodology that is based on the system stability and the disturbance rejection ability is shown.

A. Compensator Principle

The compensator block provides the compensation current $i_{q_{\mathrm{COM}}}$. Then, the modified q-axis current reference $i_{q_M}^{\mathrm{Ref}}$ is obtained by subtracting the compensation current $i_{q_{\mathrm{COM}}}$ to the main q-axis reference current i_q^{Ref} generated by the speed loop (see Fig. 1)

$$i_{q_M}^{\mathrm{Ref}} = i_q^{\mathrm{Ref}} - i_{q_{\mathrm{COM}}}. \tag{10}$$

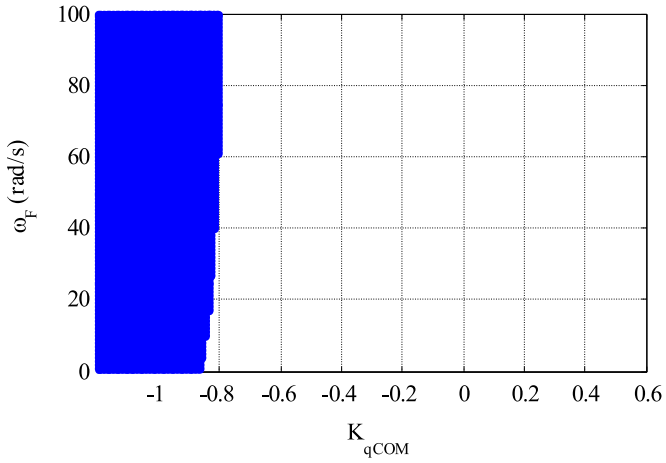

Fig. 2. Stable and unstable poles location various the compensation gain $K_{q\mathrm{COM}}$ and the filter cutoff frequency ω_F.

The proposed compensating q-axis effort is calculated through the use of a high-pass filter and a weighting factor

$$i_{q\mathrm{COM}} = \frac{s}{s+\omega_F} K_{q\mathrm{COM}}\, i_q \tag{11}$$

where $K_{q\mathrm{COM}}$ and ω_F are the compensation gain and the filter cutoff angular frequency, respectively.

The speed ripple compensator parameters $K_{q\mathrm{COM}}$ and ω_F should be designed properly to generate an appropriate compensating signal at low-speed operation.

B. Compensator Design

In terms of the Laplace transform, the relation between the system output ω_E, the system input ω_E^{Ref}, and the disturbance Γ_L is given as

$$\omega_E = H(s)\omega_E^{\mathrm{Ref}} - S(s)\Gamma_L \tag{12}$$

where $H(s)$ is the closed-loop transfer function and $S(s)$ is the sensitivity function. The expressions of $H(s)$ and $S(s)$ are given in the Appendix.

Note that, in Fig. 1, the converter is modeled as a simple gain, and since the compensator is devoted to deal with low-frequency harmonics, it is assumed that delay times due to the pulse width modulation and the digital implementation of the control loops are negligible and do not influence the design of the proposed compensator.

To evaluate the influence of the induced signal in the system stability, the evolution of the closed-loop transfer function poles versus the compensating gain $K_{q\mathrm{COM}}$ and the cutoff pulsation ω_F is analyzed. Fig. 2 shows whether the system stability is satisfied (white area) or not (blue area). It is observed that positive q-axis gains do not excite the system stability. It can also be noted that for compensation gain $K_{q\mathrm{COM}}$ around -0.8, the system stability slightly depends on the filter cutoff frequency value.

Fig. 3(a) and (b) shows the Bode magnitude plots of the sensitivity function $S(s)$ versus the cutoff pulsation ω_F and the compensation gain $K_{q\mathrm{COM}}$, respectively. Fig. 3(a) illustrates the influence of the cutoff pulsation ω_F in the Bode magnitude of

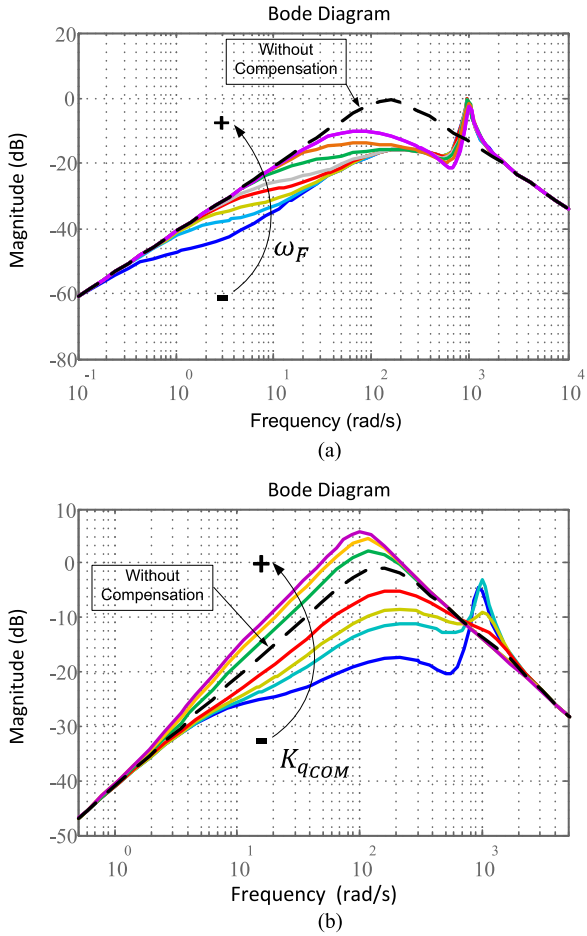

Fig. 3. Bode magnitude plots of the sensitivity function $S(s)$ for (a) $K_{q\mathrm{COM}} = -0.8$ and ω_F (0.5–50 rad/s), and (b) $\omega_F = 10$ rad/s and $K_{q\mathrm{COM}}$ (-0.83 to 1.2).

the sensitivity function $S(s)$ when the compensation gain is set to -0.8. It can be observed that the damping capability is more significant for low values of the cutoff pulsation ω_F. Fig. 3(b) shows the evolution of the sensitivity function $S(s)$ magnitude when the compensation gain $K_{q\mathrm{COM}}$ is changed from -0.83 to 1.2 and the filter angular frequency is set to 10 rad/s. According to this result, it can be concluded that for angular frequencies between 10 and 650 rad/s, the disturbance rejection is more significant for lower negative gains. Positive compensation gains increase the magnitude of the sensitivity function compared to the case where $K_{q\mathrm{COM}} = 0$ (without compensation). For angular frequencies above 800 rad/s, which is above the nominal angular frequency of the studied PMSM (2π 100 rad/s), the compensator increases the speed ripple magnitude.

The study of the parameters sensitivity refers to the robustness of the proposed speed ripple compensator under modeling uncertainties and operating parameter changes. The compensator parameters are set to $K_{q\mathrm{COM}} = -0.8$ and $\omega_F = 10$ rad/s.

Fig. 4 shows that the system remains stable even with 50% uncertainties on the stator inductance L_s and the stator resistance R_s.

To conclude with, the best compensator gains are to be selected in manner to obtain the highest disturbance rejection

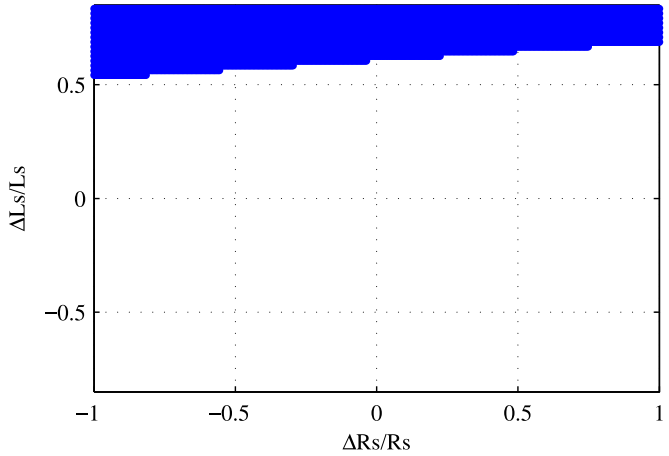

Fig. 4. Stability robustness analysis as a function of relative variations on the stator inductance L_s and the stator resistance R_s.

ability and where the system stability and robustness are guaranteed.

IV. Simulation Results

In order to check the proposed design, simulations have first been carried out using MATLAB/ Simulink. In this test, a non-sinusoidal flux density distribution is simulated by using (9), and the sixth and 12th torque components are chosen equal to 6% and 2% of the rated torque, respectively. The performance criterion to evaluate the effectiveness of the proposed scheme for speed ripple reduction is the speed ripple factor (SRF). It is usually assessed as a percentage of deviation from the rated value [6]

$$\text{SRF} = \frac{\omega_{\text{pk-pk}}}{\omega_E^{\text{Ref}}} 100(\%) \tag{13}$$

where $\omega_{\text{pk-pk}}$ is the peak-to-peak speed ripples and ω_E^{Ref} is the reference speed.

Fig. 5(a) shows the evolution of the SRF versus both the compensation gain $K_{q_{\text{COM}}}$ and the cutoff pulsation ω_F.

Fig. 5(b) illustrates the influence of the compensation gain $K_{q_{\text{COM}}}$ on the SRF evolution. This result shows that the disturbance rejection ability is more significant for lower negative gains, i.e., the SRF is reduced from 12.6% for $K_{q_{\text{COM}}} = 0$ to 6.1% for $K_{q_{\text{COM}}} = -0.8$ and $\omega_F = 10$ rad/s. It can also be noted that positive compensation gains lead to the SRF increase, i.e., the SRF changes from 12.6% for $K_{q_{\text{COM}}} = 0$ to 13.7% for $K_{q_{\text{COM}}} = +0.8$ and $\omega_F = 10$ rad/s. Fig. 5(c) shows the SRF changes versus the cutoff pulsation ω_F. Herein, speed ripples are reduced for low cutoff pulsations especially around $\omega_F = 10$ rad/s. Note that the provided simulation results are in accordance with the selected compensator parameters in the theoretic design part.

Fig. 6(a) and (b) shows the speed response in the time domain, respectively, at 30 and 50 r/min under 10-N·m load torque without and with the proposed speed ripple compensator. The figure is illustrated in two sequences, respectively, from 0.5 to 1 s without compensation and between 1 and 1.5 s with the proposed compensator. These results show that speed ripples are reduced after activating the proposed compensator at $t = 1$ s.

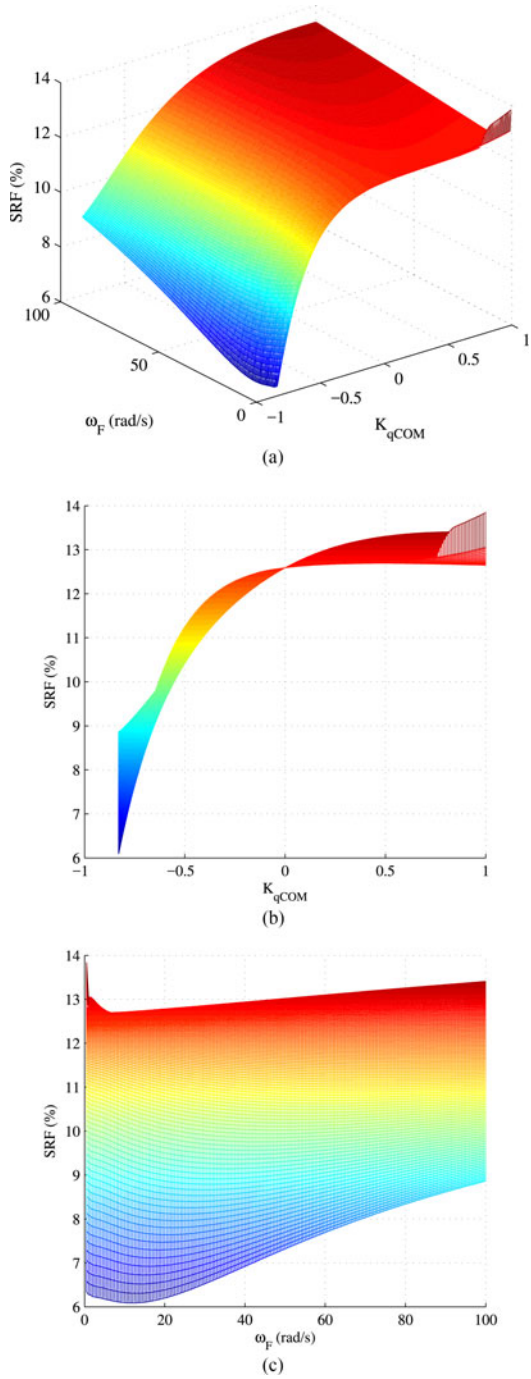

Fig. 5. Evolution of the SRF versus (a) the compensation gain $K_{q_{\text{COM}}}$ and the filter cutoff frequency ω_F, (b) the compensation gain $K_{q_{\text{COM}}}$, and (c) the filter cutoff frequency ω_F.

V. Experimental Results

To check the validity of the proposed speed ripple compensator, experiments have also been carried out. The experimental hardware setup is shown in Fig. 7. The test bench consists of a PMSM and a dc generator used as a load. The proposed control is implemented in a dSPACE DS1103PPC. Parameters of the

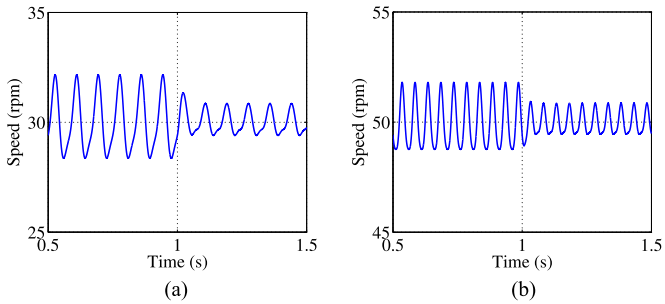

Fig. 6. Simulated speed behavior before and after compensation under 10-N· m load torque. (a) Speed at 30 r/min. (b) Speed at 50 r/min.

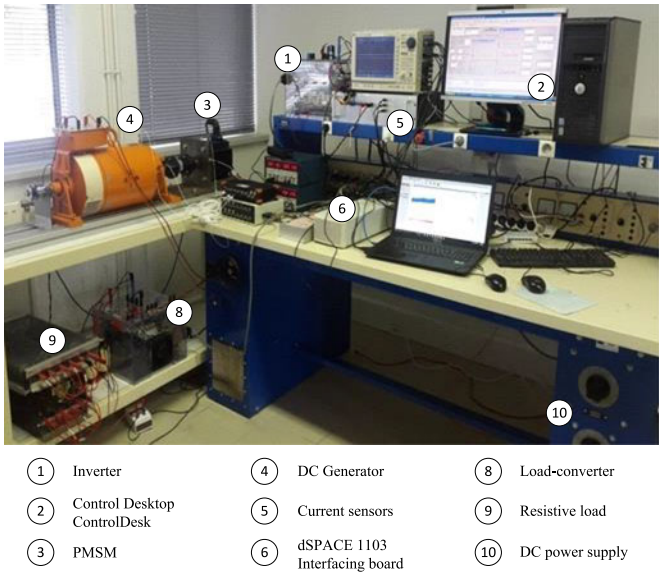

Fig. 7. Experimental test bench.

PMSM drive are listed in Table I. To highlight the improvement of the proposed technique, a comparison with an ILC implemented in the time domain is proposed. The ILC controller scheme and the parameter design are provided in [17]. The used learning gains are $\Phi = 0.45$, $\Gamma = 0.02$, and $\alpha = 0.1$.

Fig. 8(a) and (b) illustrates the steady-state behavior of the speed response, respectively, before and after activating the ILC method and the proposed speed ripple compensator. The operating conditions are a speed 0.02 p.u. (30 r/min) and a load torque 0.6 p.u. (10 N·m). It is shown that the speed ripples are reduced after activating the compensation algorithms. The SRF rates are decreased from 20.83% without compensation to 12.33% with the ILC method and to 10.7% with the proposed method. The harmonic spectrums of without and with the compared compensation algorithms are given in Fig. 8(c) and (d). It can be seen that peaks appear at specific harmonic orders, especially one, two, and six times of the fundamental electrical frequency. It can also be seen that some noninteger harmonics are present in the speed waveforms, i.e., [4.5th (9 Hz) and 5.5th harmonics (11 Hz)]. When the sixth and 12th harmonics components can be related to the nonsinusoidal flux density distribution in the air gap, the first and second and the other noninteger harmonic components are introduced by the coupling mechanical load. The compensation methods allow reducing harmonic peaks, which occur without

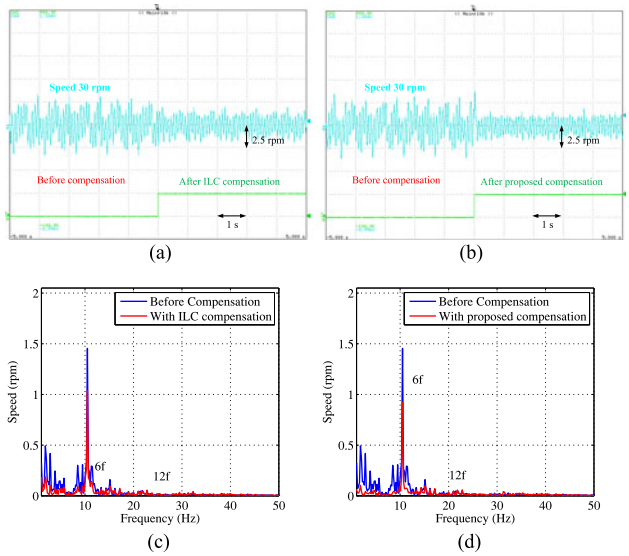

Fig. 8. Speed behavior at 30-r/min 10-N· m load torque before and after activating compared compensation methods, respectively: the ILC method and the proposed method. (a) and (b) Time domain. (c) and (d) Frequency domain.

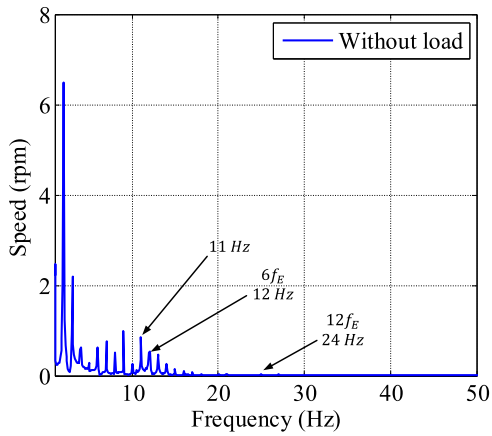

Fig. 9. Speed spectrum at 30 r/min under no external load torque without compensation.

compensation. Also, it should be noted that the low-frequency harmonics are more damped with the proposed method.

To highlight the effect of the coupling dc generator in the apparition of low-order harmonics, Fig. 9 shows the frequency spectra at speed 0.02 p.u. (30 r/min) under no external load torque. This result illustrates that the described low-order harmonics in Fig. 8(c) and (d) are induced by the nonideal load mechanism. By comparison to Fig. 8(c) and (d), it can be noted that the magnitude of the low-order harmonics are fairly damped under loading conditions.

Fig. 10 shows time and harmonic spectrum of the speed response, respectively, before and after activating the ILC method and the proposed speed ripple compensator. The operating conditions are a speed 0.0333 p.u. (50 r/min) and a load torque 0.6 p.u. (10 N·m). The SRF when a PI controller is applied without compensation is 12.8% and is reduced to 7% with ILC method and to 5.5% with the proposed method. As in Fig. 8(b), Fig. 10(c) and (d) shows clearly that the speed harmonics contain specific harmonic orders. It is noteworthy that the proposed

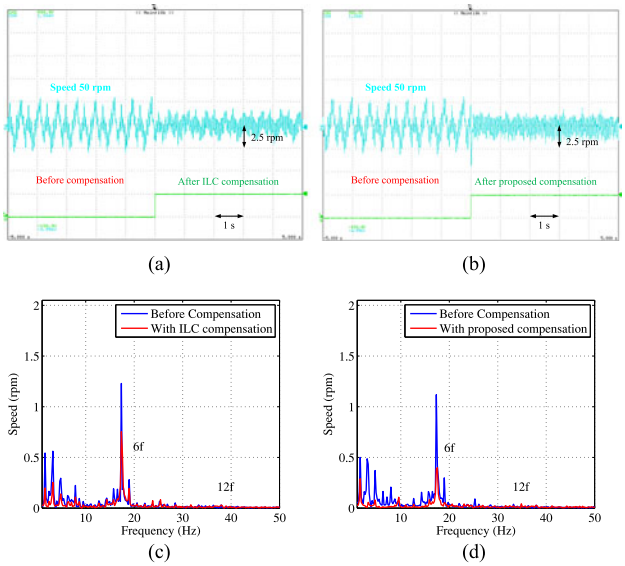

Fig. 10. Speed behavior at 50-r/min 10-N·m load torque before and after activating compared compensation methods, respectively: the ILC method and the proposed method. (a) and (b) Time domain. (c) and (d) Frequency domain.

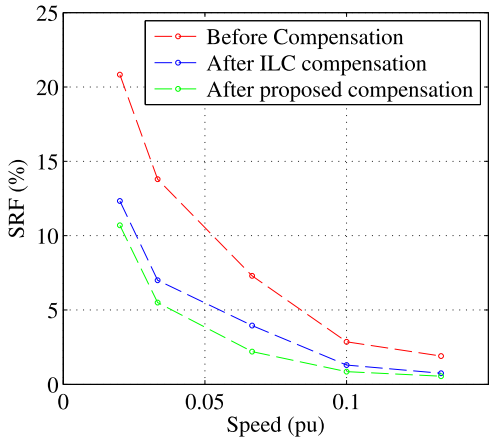

Fig. 11. Evolution of the SRF at different speeds under 10 N·m: before compensation (red), after ILC compensation (blue), and after proposed compensation (green).

speed ripple compensator is more efficient than the ILC method especially for harmonics below ten times of fundamental electrical frequency.

To summarize the reduction rate in speed ripples under low-speed working conditions, SRF values before and after compensation for different speed values are shown in Fig. 11. The load torque is set to 10 N·m. From this result, it can be seen that the speed ripples decrease when the speed increases. The high-frequency ripples are removed by the load inertia. Compared to the ILC method, the SRF evolution indicates that ripples are more reduced with the proposed method especially at very low speed operation.

To illustrate the behavior of the ILC method and the proposed method under different operating conditions, Fig. 12 shows the speed and the q-axis current responses. In this experiment, first, the speed is changed from 50 to 60 r/min under 10-N·m load. Second, a load torque from 10 to 15 N·m is applied. Under steady-state conditions, Fig. 12(a), where PI control is applied

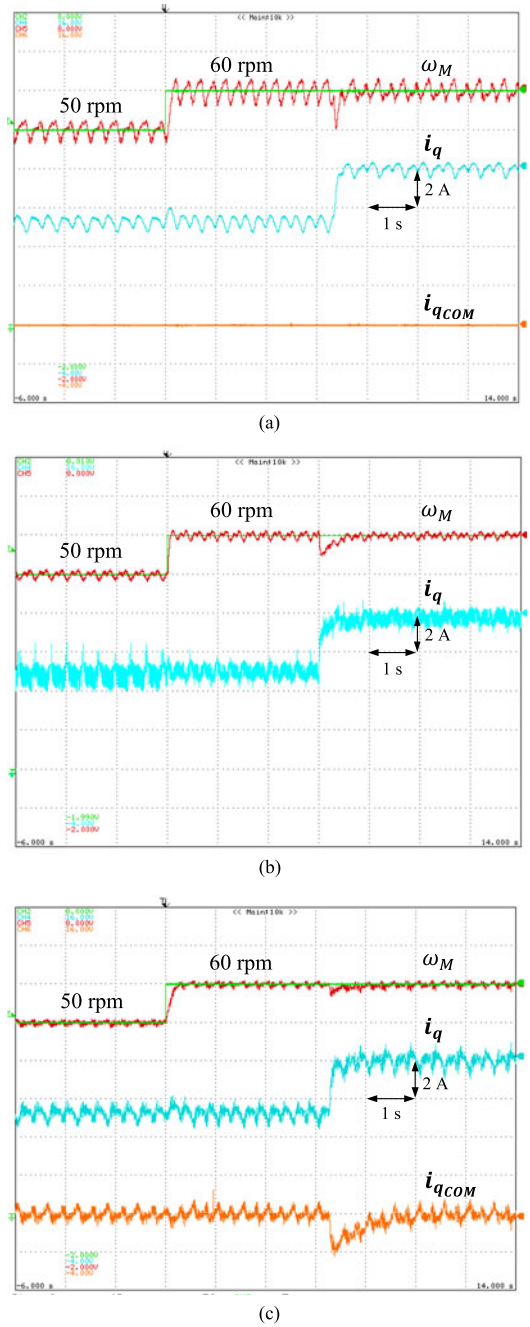

Fig. 12. Experimental measurements of the speed response and the q-axis current. (a) Without compensation. (b) With ILC compensation. (c) With the proposed compensation.

without compensation, shows that there are ripples in the speed waveform and the use of ILC method [see Fig. 12(b)] and the proposed compensator [see Fig. 12(c)] allows reducing these ripples. Regarding the current waveform, there are additional ac components in the waveform of the q-axis current when the compensation methods are activated. Speed droop occurs during the load step, and the corresponding droop rates are, respectively, 16.67% without compensation, 8.33% with ILC method, and only 5% with the proposed compensator. In terms of dynamic performance, perturbation rejection times are about 0.55 s with the ILC method and about 0.4 s with the proposed compensator. However, when speed is moved from 50 to

60 r/min, the speed response with the proposed method is slower (0.25 s) than with the ILC method (0.12 s).

VI. Conclusion

This paper proposed a simple and effective compensation method to ensure speed smoothness at low-speed operation of PMSM drives. The proposed approach is based on the generation of a compensation signal, which is added to the main quadratic-current reference in such a way that the undesired ripples are rejected by the controller. The design process of the proposed compensator is detailed. It takes the local stability of the system and the disturbance rejection ability into account. A comparison with the ILC method shows that the proposed compensator allows us to reduce speed ripples at the steady state and the speed performance is less impacted by load changes.

The proposed approach can be easily added to a classical FOC without extra computational cost and can be extended to other PMSM drives where low-order harmonics are undesired.

Appendix

The system parameters are listed in Table I.

TABLE I
System Parameters

PMSM Parameters	Value
Stator resistance	0.25 Ω
Stator inductance	4.8 mH
Number of the pole pairs	4
Magnet flux	0.32 Wb
Inertia (PMSM with driven load)	0.00774 kg·m^2
Frictional coefficient	0.0089 N·m/s
Nominal speed	1500 r/min
Control parameters	Value
Inner loop cutoff frequency ω_c	1500 rad/s
Outer loop cutoff frequency ω_w	100 rad/s

The closed loop transfer function $H(s)$ and the sensitivity function $S(s)$ are as follows:

$H(s) = \mathrm{Num}_H(s)/\mathrm{Den}(s)$

$S(s) = \mathrm{Num}_S(s)/\mathrm{Den}(s)$

with

$\mathrm{Num}_H(s) = (K_{pC}K_{p\omega}p^2\psi_{\mathrm{PM}})s^3 + (K_{iC}K_{p\omega}p^2\psi_{\mathrm{PM}} + K_{i\omega}K_pip^2\psi_{\mathrm{PM}} + K_{pC}K_{p\omega}p^2\psi_{\mathrm{PM}}\omega_F)s^2 + (K_{iC}K_{i\omega}p^2\psi_{\mathrm{PM}} + K_{iC}K_{p\omega}p^2\psi_{\mathrm{PM}}\omega_F + K_{i\omega}K_{pC}p^2\psi_{\mathrm{PM}}\omega_F)s + K_{iC}K_{i\omega}p^2\psi_{\mathrm{PM}}\omega_F$

$\mathrm{Num}_S(s) = (L_sp)s^4 + (K_{pC}p + pR_s + K_{pC}K_{q\mathrm{COM}}p + L_sp\omega_F)s^3 + (K_{iC}p + K_{iC}K_{q\mathrm{COM}}p + K_{pC}p\omega_F + pR_s\omega_F)s^2 + (K_{iC}p\omega_F)s$

$\mathrm{Den}(s) = (J_ML_s)s^5 + (L_sF_M + J_MR_s + J_MK_{pC} + J_MK_{pC}K_{q\mathrm{COM}} + J_ML_s\omega_F)s^4 + (K_{pC}K_{p\omega}\psi_{\mathrm{PM}}p^2 + K_{pC}F_M + F_MR_s + J_MK_{iC} + J_MK_{iC}K_{q\mathrm{COM}} + K_{pC}K_{q\mathrm{COM}}F_M + J_MK_{pC}\omega_F + L_sF_M\omega_F + J_MR_s\omega_F)s^3 + (K_{iC}F_M + K_{iC}K_{q\mathrm{COM}}F_M + J_MK_{iC}\omega_F + K_{pC}F_M\omega_F + F_MR_s\omega_F + K_{iC}K_{p\omega}p^2\psi_{\mathrm{PM}} + K_{i\omega}K_{pC}p^2\psi_{\mathrm{PM}} + K_{pC}K_{p\omega}p^2\psi_{\mathrm{PM}}\omega_F)s^2 + (K_{iC}F_M\omega_F + K_{iC}K_{i\omega}p^2\psi_{\mathrm{PM}} + K_{iC}K_{p\omega}p^2\psi_{\mathrm{PM}}\omega_F + K_{i\omega}K_{pC}p^2\psi_{\mathrm{PM}}\omega_F)s + K_{iC}K_{p\omega}p^2\psi_{\mathrm{PM}}\omega_F.$

References

[1] P. Pillay, "Control characteristics and speed controller design for a high performance permanent magnet synchronous motor drive," *IEEE Trans. Power Electron.*, vol. 5, no. 2, pp. 151–159, Apr. 1990.

[2] T. M. Jahns and W. L. Soong, "Pulsating torque minimization techniques for permanent magnet AC motor drives—A review," *IEEE Trans. Ind. Electron.*, vol. 43, no. 2, pp. 321–330, Apr. 1996.

[3] C. C. Chan, J. Z. Jiang, G. H. Chen, X. Y. Wang, and K. T. Chau, "A novel polyphase multipole square-wave permanent magnet motor drive for electric vehicles," *IEEE Trans. Ind. Appl.*, vol. 30, no. 5, pp. 1258–1266, Sep./Oct. 1994.

[4] A. Gebregergis *et al.*, "Modeling of permanent-magnet synchronous machine including torque ripple effects," *IEEE Trans. Ind. Appl.*, vol. 51, no. 1, pp. 232–239, Jan./Feb. 2015.

[5] S. K. Panda and Xu, and W. Q. W. Qian, "Review of torque ripple minimization in PM synchronous motor drives," *Proc. IEEE Power Energy Soc. Gen. Meeting Convers. Del. Elect. Energy 21st Century*, 2008, pp. 1–6.

[6] W. Qian, S. Panda, and J. Xu, "Speed ripple minimization in PM synchronous motor using iterative learning control," *IEEE Trans. Energy Convers.*, vol. 20, no. 1, pp. 53–61, Mar. 2005.

[7] C. Xia, B. Ji, and Y. Yan, "Smooth speed control for low-speed high-torque permanent-magnet synchronous motor using proportional-integral-resonant controller," *IEEE Trans. Ind. Electron.*, vol. 62, no. 4, pp. 2123–2134, Apr. 2015.

[8] S. Chai, L. Wang, and E. Rogers, "A cascade MPC control structure for a PMSM with speed ripple minimization," *IEEE Trans. Ind. Electron.*, vol. 60, no. 8, pp. 2978–2987, Aug. 2013.

[9] Y. Cho, S. Member, T. Labella, and S. Member, "A three-phase current reconstruction strategy with online current offset compensation," *IEEE Trans. Ind. Electron.*, vol. 59, no. 7, pp. 2924–2933, Jul. 2012.

[10] Y. Cho, K.-b. Lee, S. Member, J.-H. Song, and Y. I. Lee, "Torque-ripple minimization and fast dynamic scheme for torque predictive control of permanent-magnet synchronous motors," *IEEE Trans. Power Electron.*, vol. 30, no. 4, pp. 2182–2190, Apr. 2015.

[11] Y. Xu, N. Parspour, and U. Vollmer, "Torque ripple minimization using online estimation of the stator resistances with consideration of magnetic saturation," *IEEE Trans. Ind. Electron.*, vol. 61, no. 9, pp. 5105–5114, Sep. 2014.

[12] B. N. Nakao and K. Akatsu, "Suppressing pulsating torques: Torque ripple control for synchronous motors," *IEEE Ind. Appl. Mag.*, vol. 20, no. 6, pp. 33–44, Nov./Dec. 2014.

[13] D. Flieller, N. K. Nguyen, P. Wira, G. Sturtzer, D. Ould, and J. Merckl, "A self-learning solution for torque ripple reduction for non-sinusoidal permanent magnet motor drives based on artificial neural networks," *IEEE Trans. Ind. Electron.*, vol. 61, no. 2, pp. 655–666, Feb. 2014.

[14] J. Lara, J. Xu, and A. Chandra, "Effects of rotor position error in the performance of field oriented controlled PMSM drives for electric vehicle traction applications," *IEEE Trans. Ind. Electron.*, vol. 63, no. 8, pp. 4738–4751, Aug. 2016.

[15] K. Jezernik, J. Korelic, and R. Horvat, "PMSM sliding mode FPGA-based control for torque ripple reduction," *IEEE Trans. Power Electron.*, vol. 28, no. 7, pp. 3549–3556, Jul. 2013.

[16] P. Beccue, J. Neely, S. Pekarek, and D. Stutts, "Measurement and control of torque ripple-induced frame torsional vibration in a surface mount permanent magnet machine," *IEEE Trans. Power Electron.*, vol. 20, no. 1, pp. 182–191, Jan. 2005.

[17] W. Qian, S. Panda, and J.-X. Xu, "Torque ripple minimization in PM synchronous motors using iterative learning control," *IEEE Trans. Power Electron.*, vol. 19, no. 2, pp. 272–279, Mar. 2004.

[18] Y.-S. Choi, H. H. Choi, and J.-W. Jung, "Feedback linearization direct torque control with reduced torque and flux ripples for IPMSM drives," *IEEE Trans. Power Electron.*, vol. 31, no. 5, pp. 3728–3737, May 2016.

[19] G. H. Foo and X. Zhang, "Constant switching frequency based direct torque control of interior permanent magnet synchronous motors with reduced ripples and fast torque dynamics," *IEEE Trans. Power Electron.*, vol. 31, no. 9, pp. 6485–6493, Sep. 2016.

[20] A. Mora, A. Orellana, J. Juliet, and R. Cardenas, "Model predictive torque control for torque ripple compensation in variable speed PMSMs." *IEEE Trans. Ind. Electron.*, vol. 63, no. 7, pp. 4584–4592, Jul. 2016.

[21] Y. Cho, K. B. Lee, J. H. Song, and Y. I. Lee, "Torque-ripple minimization and fast dynamic scheme for torque predictive control of permanent-magnet synchronous motors," *IEEE Trans. Power Electron.*, vol. 30, no. 4, pp. 2182–2190, Apr. 2015.
[22] Y. Yuan, F. Auger, L. Loron, S. Moisy, and M. Hubert, "Torque ripple reduction in permanent magnet synchronous machines using angle-based iterative learning control," in *Proc. 38th Annu. Conf. IEEE Ind. Electron. Soc.*, Oct. 2012, pp. 2507–2512.
[23] A. Houari, F. Auger, J.-C. Olivier, and M. Machmoum, "A new compensation technique for PMSM torque ripple minimization," in *Proc. IEEE Ind. Appl. Soc. Annu. Meeting*, Addison, TX, USA, 2015, pp. 1–6.
[24] S. Chen, C. Namuduri, and S. Mir, "Controller-induced parasitic torque ripples in a PM synchronous motor," *IEEE Trans. Ind. Appl.*, vol. 38, no. 5, pp. 1273–1281, Sep./Oct. 2002.

Azeddine Houari received the engineer degree from Béjaïa University, Béjaïa, Algeria, in 2008, and the Ph.D. degree from the University of Lorraine, Nancy, France, in 2012, both in electrical engineering.

Since 2014, he has been an Assistant Professor with the University of Nantes, Nantes, France. He exercises his research activities with the Institut de Recherche en Énergie Électrique de Nantes Atlantique, Saint-Nazaire, France. His current research deals with power quality and stability issues in stationary and embedded dc and ac microgrids.

Ahmed Bouabdallah received the engineering degree from National Polytechnic Institute, Algiers, Algeria, in 2010, and the Ph.D. degree from the University of Nantes, Nantes, France, in 2014, both in electrical engineering.

He is currently with the Institut de Recherche en Énergie Électrique de Nantes Atlantiques, Saint-Nazaire, France. His research interests include integration and sizing issues in fuel-cell-, battery-, and photovoltaic-based systems, and control of multiphase drives.

Ali Djerioui was born in M'sila, Algeria, in 1986. He received the engineering degree in electrical engineering from the University of M'sila, M'sila, in 2009; the M.Sc. degree in electrical engineering from Polytechnic Military Academy, Algiers, Algeria, in 2011; and the doctorate degree in electronic instrumentation systems from the University of Science and Technology, Houari Boumediene, Algiers, in 2016.

He is currently an Assistant Professor with the University of Mohamed Boudiaf, M'sila. His current research interests include power electronics, control, microgrids, and power quality.

Mohamed Machmoum was born in Casablanca, Morocco, on November 29, 1961. He received the Diplo. Eng. degree from the Institut Supérieur Industriel de Liège, Liège, Belgium, in 1984, and the Ph.D. degree from the Institut National Polytechnique of Lorraine, Vandœuvre-lès-Nancy, France, in 1989, both in electrical engineering.

In 1991, he joined l'Ecole Polytechnique de l'Université de Nantes, Nantes, France, as an Assistant Professor, where since September 2005, he has been a Professor. He is the head of IREENA Laboratory, University of Nantes, Nantes. His main research interests include power electronics, power quality, wind or tidal energy conversion systems, and microgrids.

Francois Auger was born in Saint-Germain-en-Laye, France, in 1966. He received the engineer and D.E.A. degrees in signal processing and automatic control from the Ecole Nationale Supérieure de Mécanique de Nantes, Nantes, France, in 1988, and the Ph.D. degree in signal processing and control from the Ecole Centrale de Nantes, Nantes, in 1991.

From 1993 to 2012, he was an Assistant Professor at the Institut Universitaire de Technologie (IUT) de Saint-Nazaire, Université de Nantes, Nantes, where he is currently a Full Professor. His current research interests include automatic control of power systems, spectral analysis, and time-frequency representation.

Dr. Auger is a member of the GdR720 CNRS "Information, Signal, Images et ViSion."

Abdallah Darkawi was born in Moroni, Comoros Islands, in 1982. He received the M.Phil. degree in electrical engineering from University Cadi Ayyad, Marrakech, Morocco, in 2007, and the Ph.D. degree in electrical engineering from Université Montpellier 2, Montpellier, France, in 2013.

He is currently an Engineer with the Department of Electrical Engineering, Ecole Polytechnique de l'Université de Nantes, Nantes, France, and the IREENA Laboratory. His research interests include power electronic systems and drives, renewable energy, and energy management.

Jean-Christophe Olivier was born in Paris, France, in 1979. He received the M.S. degree from the Ecole polytechnique de l'Université de Nantes, Nantes, France, in 2004, and the Ph.D. degree from the University of Nantes, Nantes, in 2006, both in electrical engineering.

Since 2008, he has been an Assistant Professor with the Institut de Recherche en Énergie Électrique de Nantes Atlantique, Saint-Nazaire, France. His research interests include the fuel-cell system integration for transportation and the technoeconomic optimization of power systems.

Mohamed Fouad Benkhoris was born in Bou-sada, Algeria, on September 17, 1963. He received the engineer degree in electrical engineering from the Ecole Nationale Polytechnique d'Alger, El Harrach, Algeria, in 1986, and the Ph.D. degree in electrical engineering and the Habilitation à diriger des recherches from the National Polytechnic Institute of Lorraine, Vandœuvre-lès-Nancy, France, in 1991 and 2004, respectively.

Since 1991, he has been an Assistant Professor with the Department of Electrical Engineering, Polytech Nantes, Nantes, France, where he has been a Professor since 2006. He does research with the Institut de Recherche en Énergie Électrique de Nantes Atlantiques, Saint-Nazaire, France. His research interests include dynamical modeling, simulation, and control of electrical drives, and especially multiphase drive, multiconverter systems, and embarked networks.